nature catalysis

Article

https://doi.org/10.1038/s41929-023-00949-w

Blocking the sulfonate group in Nafion to unlock platinum's activity in membrane electrode assemblies

Received: 21 July 2022

Accepted: 15 March 2023

Published online: 17 April 2023

Check for updates

Fadong Chen[1], Siguo Chen[1] ✉, Aoxue Wang[2], Meng Wang[1], Lin Guo[2] ✉ & Zidong Wei[1] ✉

The specific adsorption of ionomer sulfonate groups on Pt-based catalysts in membrane electrode assemblies (MEAs) has severely restricted Pt catalytic activity, Pt utilization, proton conductivity and mass transport. Here we report a blocking strategy using cyclohexanol to mitigate the detrimental impacts of the Nafion ionomer. Cyclohexanol with a chair or boat conformation blocked the adsorption path of the ionomer onto the Pt surface via coordination with the ionomer, which released the Pt activity sites and dramatically improved the mass transport path. This MEA with cyclohexanol exhibits striking performance improvement in the kinetic and mass transport regions, along with strong stability. The proposed strategy provides a direction to tune the Pt/ionomer interface and improve the catalytic activity of Pt in MEA.

Platinum-based nanomaterials have been recognized as the most efficient catalysts for proton exchange membrane fuel cells (PEMFCs). However, their scarcity and rapidly growing cost have markedly hindered the broad application of PEMFCs[1–3]. To reduce Pt consumption in PEMFCs, many efforts have been made in recent decades to develop different low-Pt-loading catalysts with high performance. This has led to marked improvements in the catalytic activity of Pt-based catalysts for the oxygen reduction reaction (ORR)[4–6]. In previous studies, platinum–cobalt core–shell nanoparticles (LP@PF-2) derived from imidazolate frameworks have been shown to exhibit much higher mass activity (12.36 A mg_{Pt}^{-1}) relative to commercial Pt/C catalysts (0.10 A mg_{Pt}^{-1})[7]. However, this substantial improvement in catalytic activity was only observed on the rotating disk electrode (RDE) and has not yet been obtained in the corresponding membrane electrode assembly (MEA)[8–10]. The maximum power density of LP@PF-2 MEAs was only 1.29 and 1.28 times as high as that of commercial Pt/C MEAs in H_2–O_2 and H_2–air fuel cells, respectively.

The performance gap mentioned above is known to be primarily caused by the different proton and O_2 transport mechanisms[11]. On the RDE, all the Pt-based nanoparticles are soaked in a liquid electrolyte and can be fully contacted by hydrated protons and dissolved O_2 through electrolyte transmission[12]. Unlike the RDE in liquid, the MEA has a much higher transport resistance. In a conventional catalyst layer, proton transport is tied down to the perfluorinated sulfonic acid (PFSA) ionomer layer (such as Nafion) covering the catalyst surface[13], and the gaseous O_2 gradually permeates through the covering ionomer layer (<10 nm thick) to reach the Pt surface[14]. The strong adsorption of the sulfonate group on the Pt surfaces restricts the side chain of the Nafion ionomer and thus decreases the microphase separation of the ionomer, leading to a further increase in mass transport resistance[15–17]. Also, the sulfonate group can badly poison Pt sites and dramatically reduce the mass activity of Pt up to a factor of 2 to 4, eventually leaving only ~20% available Pt surface[18–20]. These conditions make it difficult for Pt catalysts to achieve high performance in an MEA. To overcome the obstacles in the catalyst layer of the MEA, efforts have been made such as embedding Pt nanoparticles into porous carbon to avoid direct contact between the Pt and Nafion ionomer[20,21], introducing a ring-structured perfluoro-(2,2-dimethyl-1,3-dioxole) (PDD) or perfluoro-(2-methylene-4-methyl-1,3-dioxolane) (PFMMD) matrix into the ionomer backbone to reduce the oxygen transport resistance[22,23], achieving an

[1]The State Key Laboratory of Power Transmission Equipment & System Security and New Technology, College of Chemistry and Chemical Engineering, Chongqing University, Chongqing, China. [2]State Key Laboratory of Catalytic Materials and Reaction Engineering, SINOPEC Research Institute of Petroleum Processing Co., Beijing, China. ✉e-mail: csg810519@126.com; guolin.ripp@sinopec.com; zdwei@cqu.edu.cn

ionomer-lean Pt surface by means of a molecular masking strategy to decrease the ionomer population on the Pt surface[24,25], and optimizing the Pt/ionomer interface using ionic liquids via non-covalent interactions to tune the ORR kinetics[26–28]. Unfortunately, these strategies have important limitations in terms of comprehensively solving the barriers mentioned above, for example, part of the Pt nanoparticles into porous carbon inevitably losing the proton and oxygen transport channels, PDD or PFMMD matrix and the molecular masking strategy undoubtedly putting part of the Pt active sites in direct contact with the sulfonate group. It is clear that eliminating the detrimental effects of the ionomer layer on Pt to release the performance of Pt in MEA entirely is a big challenge.

In this article we present a blocking strategy to boost the performance of Pt-based catalysts in the MEA. The ring-structured cyclohexanol plays a critical role in constructing the blocking path. The hydroxyl oxygen of cyclohexanol connects with the sulfonate hydrogen of the ionomer by a coordination interaction, which successfully separates the sulfonate group from the Pt surface and releases more active sites of Pt. The hydroxyl hydrogen of cyclohexanol is activated, increasing the proton transport channel without losing the proton transport capability of the sulfonate group. Cyclohexanol with a chair or boat conformation also embeds among the ionomer chains, creating a non-contact Pt/ionomer space and facilitating O_2 permeability in the catalyst layer. Based on these improvements, the sulfonate group coverage on the Pt surface decreased to only 7% in the catalyst layer with cyclohexanol, much lower than that in the catalyst layer with only Nafion ionomer (21%). The as-prepared MEA with cyclohexanol exhibited a substantial performance enhancement in the kinetic region and showed far better mass transport compared to the MEA with only Nafion ionomer in the fuel cell tests. Most importantly, cyclohexanol incorporated in Nafion ionomer displayed remarkable stability after long-term constant-potential testing and 30,000 potential scanning cycles in the corresponding MEA. This study thus demonstrates that the blocking strategy is a promising way of releasing the catalytic activity of Pt and improving mass transport in the catalyst layer.

Results

Structural characterization

To investigate the interaction between Nafion and cyclohexanol, ^{1}H NMR spectra were obtained[29]. As shown in Fig. 1b, the hydroxyl hydrogen of the cyclohexanol-Nafion ionomer mixture exhibits upfield displacement (3.97 ppm) relative to pure cyclohexanol (4.36 ppm), implying that the hydroxyl hydrogen of the cyclohexanol-Nafion ionomer has a chemical environment similar to that of the sulfonate group (3.92 ppm). The upfield displacement should stem from the coordination interaction between lone-pair electrons of the hydroxyl group and the proton of the sulfonate group, which results in the formation of oxonium salt ($COH_2^+SO_3^-$) and the shielding effect on the hydrogen atoms of $-OH_2^+$ in the cyclohexanol-Nafion ionomer (Fig. 1a). Such an interaction was also detected using attenuated total reflectance-Fourier transform infrared (ATR-FTIR) spectroscopy (Fig. 1c and Supplementary Fig. 1)[30,31]. To avoid the interference of solvents from the Nafion ionomer, a dry Nafion HP membrane was chosen for ATR-FTIR measurements. As shown in Fig. 1c, the stretching vibration peak (3,403 cm^{-1}) of the hydroxyl group in the cyclohexanol-Nafion HP membrane shows a blueshift and a redshift relative to those of cyclohexanol (3,322 cm^{-1}) and Nafion HP membrane (3,484 cm^{-1}), respectively.

To investigate the interaction between the hydroxyl group and the sulfonate group in more detail, high-resolution X-ray photoelectron spectroscopy (XPS) signals of C 1*s* were deconvoluted into the corresponding components, as shown in Fig. 1d. Comparing the C 1*s* XPS peaks of cyclohexanol-Pt/C, Nafion ionomer-Pt/C and cyclohexanol-Nafion ionomer-Pt/C, a peak was observed at ~289.50 eV in cyclohexanol-Nafion ionomer-Pt/C (Fig. 1d). The peak can be attributed to the positive shift of the C–O peak of cyclohexanol due to electron transfer from C–OH to the sulfonate group. This assertion was corroborated by the negative shift of the S 2*p* binding energy of cyclohexanol-Nafion ionomer-Pt/C from 169.0 to 168.44 eV (Supplementary Fig. 2). Based on the above results and analysis, the sulfonate group is probably blocked by the hydroxyl group of cyclohexanol through formation of the $COH_2^+SO_3^-$ group. To directly explore the effect of the $COH_2^+SO_3^-$ group on Pt, the XPS signals of Pt 4*f* were collected. As shown in Fig. 1e, the Pt $4f_{7/2}$ peak (71.71 eV) of cyclohexanol-Nafion ionomer-Pt/C marginally shifted to a high binding energy compared to that of the commercial Pt/C catalyst (71.65 eV), implying that the vast majority of the sulfonate group was blocked by cyclohexanol and that the $COH_2^+SO_3^-$ group had no apparent effect on Pt. In contrast, the Pt $4f_{7/2}$ peak (71.86 eV) of Nafion ionomer-Pt/C exhibited a much higher binding energy than the other two catalyst layers. These results demonstrate that the formation of $COH_2^+SO_3^-$ groups can effectively avoid the strong adsorption of sulfonate groups on Pt and should provide a large benefit to increasing the performance of cyclohexanol-Nafion ionomer-Pt/C, as discussed later in this article.

Microphase separation of PFSA ionomers occupies an important position in the gas permeability of an MEA[32]. To describe the effect of cyclohexanol on the microphase separation of the Nafion ionomer, synchrotron small-angle X-ray scattering (SAXS) measurements were taken. Dry Nafion membrane was chosen as the characterization object to avoid the influence of the uncontrollable film thickness on its microphase separation when manually casting Nafion ionomer film. As shown in Fig. 2a,c, the scattering ring and ionomer peak associated with the ionic domain swelling of the Nafion membrane are barely noticeable in the dry Nafion HP membrane. A marked scattering ring (Fig. 2b) and a well-defined ionomer peak (Fig. 2c) at ~1.5 nm^{-1} are shown in the two-dimensional (2D) SAXS pattern and SAXS line profile of the cyclohexanol-incorporated Nafion HP membrane (that is, the cyclohexanol-Nafion HP membrane), respectively[33,34]. These results suggest that the cyclohexanol enhances the microphase separation of Nafion. The enhanced microphase separation should facilitate O_2 transport in its size- and connectivity-increasing hydrophilic ionic domains. As discussed above, the sulfonate group of the ionomer was blocked by the hydroxyl group of cyclohexanol. To assess the effect of cyclohexanol on the proton transport of cyclohexanol-Nafion, we compared the in-plane proton conductivities of the Nafion HP membrane and cyclohexanol-Nafion HP membrane[35]. The cyclohexanol-Nafion HP membrane exhibited higher proton conductivity than the pristine Nafion HP membrane, as shown in Fig. 2d and Supplementary Fig. 3. In particular, the proton conductivity of the cyclohexanol-Nafion HP membrane at 25 °C is nearly twice that of the Nafion HP membrane (Supplementary Table 1). The enhanced proton conductivity indicates that the oxonium salt has successfully activated the hydroxyl hydrogen of cyclohexanol and introduced a proton transport channel without degrading the function of the sulfonate group, as shown in Fig. 1a. This assertion is supported by the substantially weakened activation energy (E_a) of proton conduction in the cyclohexanol-Nafion HP membrane (0.125 eV) relative to the Nafion HP membrane (0.186 eV) from an Arrhenius plot (Supplementary Fig. 4).

We also investigated the role of cyclohexanol in the mesostructure of the catalyst layer through a series of physical characterization experiments. As shown by dynamic light scattering (DLS), the aggregate size of the catalyst slurry in cyclohexanol-Nafion ionomer-Pt/C is near that of Nafion ionomer-Pt/C, which is ~570 nm (Supplementary Fig. 5). As shown by X-ray diffraction (XRD) and transmission electron microscopy (TEM), cyclohexanol does not affect the crystal structure and average particle size of the Pt nanoparticles (Supplementary Figs. 6 and 7). The fluorine, sulfur and platinum elements are uniformly distributed in both catalyst layers, as observed in energy-dispersive X-ray spectroscopy (EDS) elemental mappings (Supplementary Fig. 8). The cyclohexanol-Nafion ionomer-Pt/C catalyst layer has a porous surface similar to that of the conventional Nafion ionomer-Pt/C,

https://doi.org/10.1038/s41929-023-00949-w

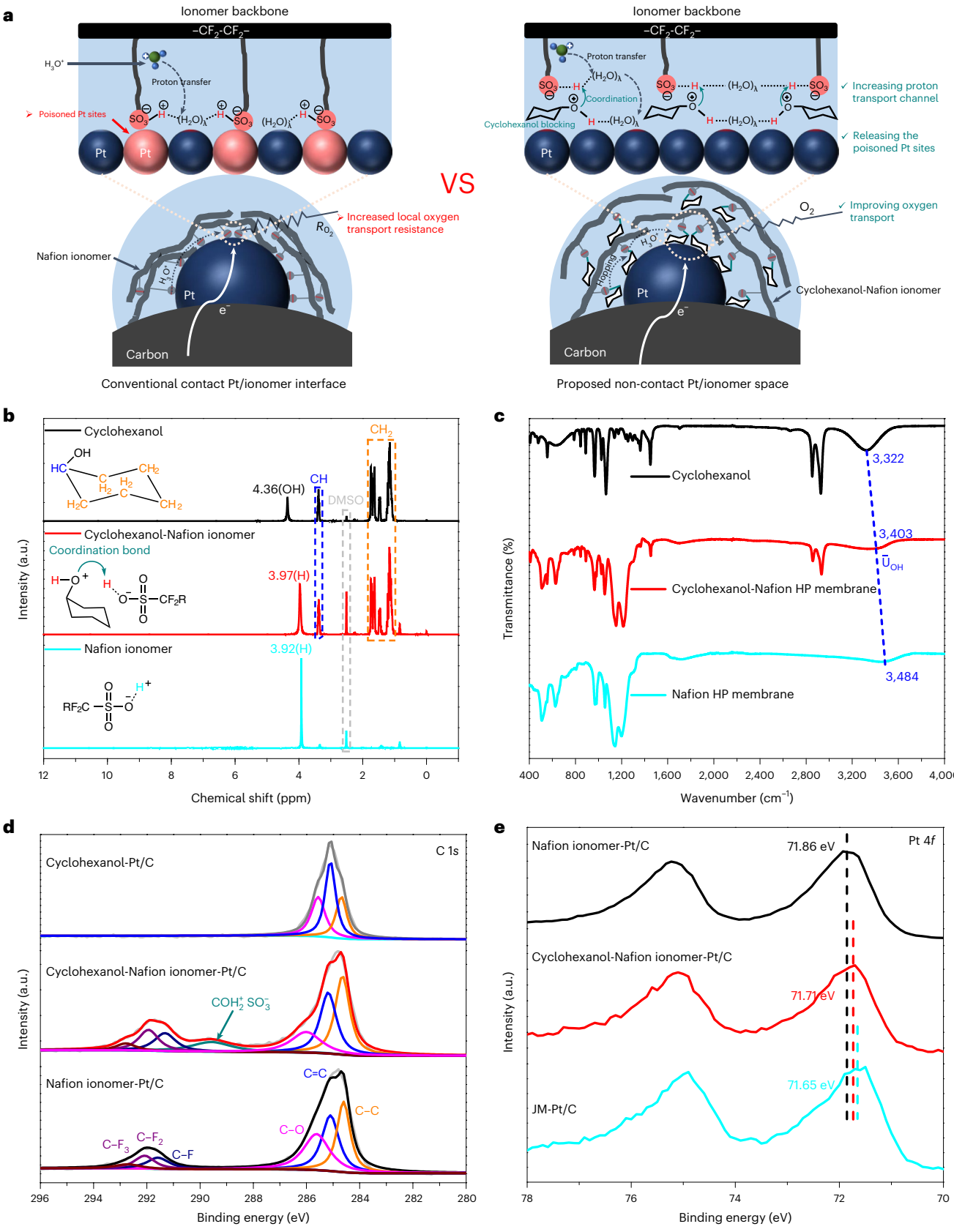

Fig. 1 | Structural characterization of cyclohexanol-Nafion. a, Illustration of the conventional direct-contact Pt/ionomer interface and the proposed non-contact Pt/ionomer space for the cathode catalyst layer. **b**, ^{1}H NMR spectra in DMSO-d_6 of cyclohexanol, cyclohexanol-Nafion ionomer and Nafion ionomer. **c**, ATR-FTIR spectra of cyclohexanol, dry cyclohexanol-Nafion HP membrane and Nafion HP membrane. **d**,**e**, C 1*s* (**d**) and Pt 4*f* (**e**) XPS spectra of Nafion ionomer-Pt/C, cyclohexanol-Nafion ionomer-Pt/C and JM-Pt/C in the practical catalyst layer (in XPS tests, the commercial Pt/C catalysts were added to monitor the real situation in the catalyst layer). The Nafion HP membrane is one of the reinforced membranes in acid form produced by DuPont. Commercial JM-Pt/C catalysts from Johnson Matthey Co. were used.

https://doi.org/10.1038/s41929-023-00949-w

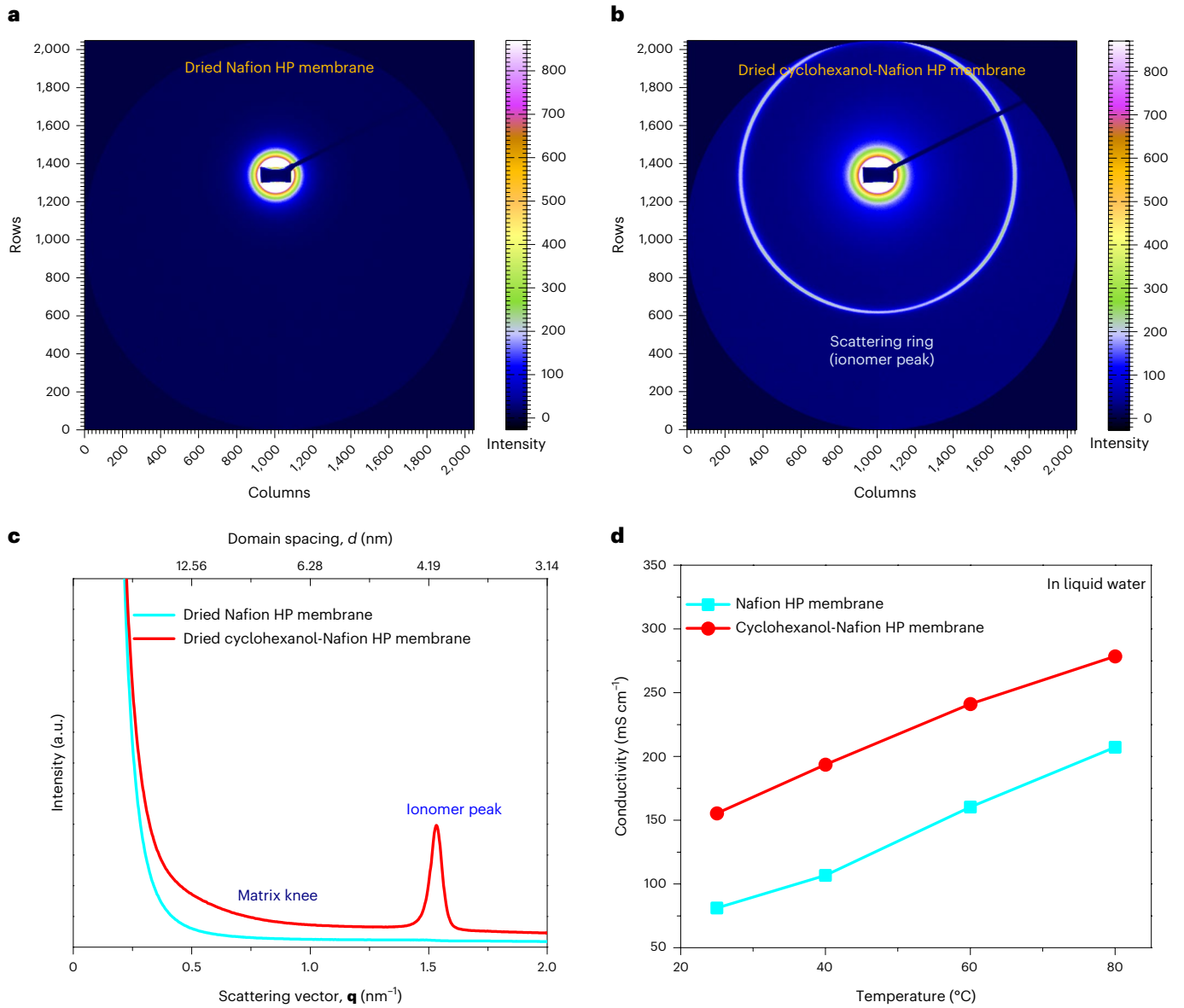

Fig. 2 | Correlation of cyclohexanol incorporation on the microphase separation and proton conductivity of Nafion membrane. a,**b**, 2D SAXS patterns of the dried Nafion HP membrane (**a**) and dried cyclohexanol-Nafion HP membrane (**b**). The colour scale representing the intensity is the same for both samples. **c**, Corresponding SAXS line profiles of the dried Nafion HP membrane and dried cyclohexanol-Nafion HP membrane were obtained by integrating the 2D SAXS patterns. **d**, In-plane proton conductivities of pristine Nafion HP and cyclohexanol-Nafion HP membranes calculated by electrochemical impedance spectroscopy (Supplementary Fig. 3) in liquid water at elevated temperatures (25 °C, 40 °C, 60 °C and 80 °C).

as shown in scanning electron microscopy (SEM) images (Supplementary Fig. 9). These results demonstrate that the cyclohexanol-Nafion ionomer-Pt/C catalyst layer features a mesostructure comparable with that of the Nafion ionomer-Pt/C catalyst layer, implying that the discrepancy in the interfacial microstructure between the catalyst layers should be the primary factor causing the difference in fuel-cell performance.

Electrochemical evaluation

To understand the effect of cyclohexanol on the electrochemical behaviour of the cyclohexanol-Nafion ionomer-Pt/C, electrochemical measurements were performed in a single cell. First, cyclic voltammogram (CV) curves of Nafion ionomer-Pt/C and cyclohexanol-Nafion ionomer-Pt/C were collected, as shown in Fig. 3a. Cyclohexanol-Nafion ionomer-Pt/C shows a similar shape to the CV curve for the Nafion ionomer-Pt/C. The same trend appeared in the other two independent tests (Supplementary Fig. 10). Both the hydrogen adsorption and desorption charges in the hydrogen underpotential deposition (H_{upd}) region were used to calculate the electrochemical surface area (ECSA)[36]. The average H_{upd}-ECSA of cyclohexanol-Nafion ionomer-Pt/C is estimated to be 46.9 $m^2\ g_{Pt}^{-1}$ (Fig. 3c), which is near that of Nafion ionomer-Pt/C (44.8 $m^2\ g_{Pt}^{-1}$). The similar H_{upd}-ECSA values verify that cyclohexanol has little effect on the protons reaching the Pt surface. More importantly, considering the absence of sulfonate-group poisoning in the H_{upd} region, this result signifies that the two catalyst layers will expose nearly the same amount of Pt sites in the kinetic control region of the fuel cell. We also performed a CO-stripping test to identify the gas permeability of Nafion ionomer-Pt/C and cyclohexanol-Nafion ionomer-Pt/C (Fig. 3b and Supplementary Fig. 11). CO is known to permeate through the ionomer layer to reach the Pt active site, and the ECSA obtained from the CO-stripping test is closely associated with the gas permeability of the ionomer layer. The cyclohexanol-Nafion

https://doi.org/10.1038/s41929-023-00949-w

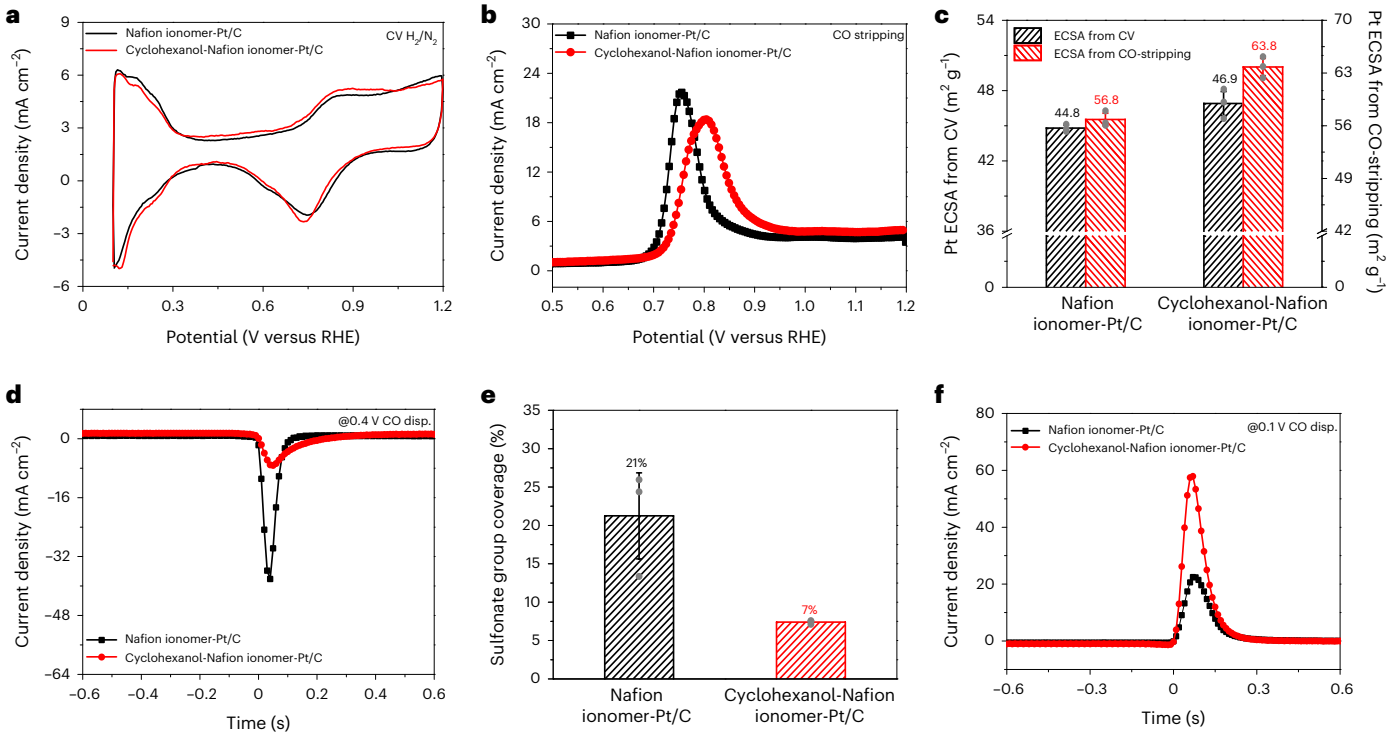

Fig. 3 | Electrochemical evaluation of the cyclohexanol-Nafion ionomer-Pt/C cathode in the fuel cell. a,**b**, CV curves (**a**) and CO-stripping curves (**b**) of the Nafion ionomer-Pt/C and cyclohexanol-Nafion ionomer-Pt/C catalyst layer. **c**, ECSA values calculated from CV curves and CO-stripping curves. **d**, CO-displacement current density–time curves measured at 0.4 V versus RHE for Nafion ionomer-Pt/C and cyclohexanol-Nafion ionomer-Pt/C catalyst layers, respectively. **e**, Sulfonate group coverage (in percent) determined from CO displacement at 0.4 V versus RHE and stripping tests for Nafion ionomer-Pt/C and cyclohexanol-Nafion ionomer-Pt/C. **f**, CO-displacement current density–time curves measured at 0.1 V versus RHE. Conditions were set as follows: 40 °C cell temperature, 100% relative humidity (RH) and ambient pressure. For the CV test, a fixed flow of 200/10 standard cubic centimetres per minute (s.c.c.m.) of H_2/N_2 was provided in the anode/cathode. For the CO-stripping and displacement tests, the gas at the cathode was switched from N_2 to CO. Error bars represent s.d. between the three independent measurements. Data are presented as mean values ± s.d.

ionomer-Pt/C (63.8 $m^2 g_{Pt}^{-1}$) shows a higher CO-stripping ECSA than the Nafion ionomer-Pt/C (56.8 $m^2 g_{Pt}^{-1}$) (Fig. 3c). This result implies that cyclohexanol dilutes the compactness of the ionomer layer and increases its gas permeability in the catalyst layer.

To quantify the Pt active sites released by cyclohexanol, CO-displacement measurements were conducted[37,38]. In this test, the sulfonate group specifically adsorbed on the Pt surface was displaced by linearly adsorbing CO, and the hydroxyl coverage on the Pt surface was neglected at 0.4 V versus the reversible hydrogen electrode (RHE)[39]. Inverted peaks can be clearly observed in Fig. 3d and Supplementary Fig. 12. The peak of cyclohexanol-Nafion ionomer-Pt/C has a much smaller area than that of Nafion ionomer-Pt/C, suggesting that markedly fewer Pt sites were occupied by the sulfonate group in cyclohexanol-Nafion ionomer-Pt/C. To intuitively compare the occupation of the sulfonate group on the Pt surfaces in the two different catalyst layers, the sulfonate-group coverage was calculated by dividing the CO-displacement charge in Fig. 3d by the corresponding CO-stripping charge in Fig. 3b ref. 40. Cyclohexanol-Nafion ionomer-Pt/C exhibited a much lower sulfonate group coverage of ~7% than Nafion ionomer-Pt/C (~21%; Fig. 3e). This result is consistent with the marginal shift of the Pt 4*f* XPS peak of cyclohexanol-Nafion ionomer-Pt/C relative to that of Pt/C. We also performed the CO-displacement experiment at 0.1 V versus RHE. As shown in Fig. 3f and Supplementary Fig. 13, the cyclohexanol-Nafion ionomer-Pt/C exhibited a larger area of CO oxidation currents than the Nafion ionomer-Pt/C, implying that the incorporation of cyclohexanol into the Nafion ionomer improved the proton transport of cyclohexanol-Nafion ionomer-Pt/C.

To investigate the catalytic activity of cyclohexanol-Nafion ionomer-Pt/C in the MEA, the single cell was tested at 80 °C with O_2 as the cathodic gas feed. For comparison, the benchmark catalyst layer (Nafion ionomer-Pt/C) of the MEA was fabricated with Nafion but without cyclohexanol (see Methods for details). The amount of cyclohexanol was optimized in the catalyst layer. As shown in Supplementary Fig. 14, the high proportion of cyclohexanol (the weight ratio for cyclohexanol/ionomer/carbon is 40/1/2.5) produces a high ohmic polarization in the fuel cell. The optimized weight ratio of cyclohexanol/ionomer/carbon was determined to be 10/1/2.5. Figure 4a shows the polarization and power-density plots of the fuel cells with Nafion ionomer-Pt/C and cyclohexanol-Nafion ionomer-Pt/C measured in H_2–O_2 conditions. The cyclohexanol-Nafion ionomer-Pt/C displayed a higher current density than the Nafion ionomer-Pt/C during polarization. The peak power density (1.804 W cm^{-2}) of cyclohexanol-Nafion ionomer-Pt/C is ~1.37 times higher than that (1.318 W cm^{-2}) of Nafion ionomer-Pt/C. These results directly confirm the improvement of the gas permeability of the ionomer layer by cyclohexanol. Figure 4b shows Tafel plots normalized for cathode Pt loading and corrected by high-frequency resistance (HFR). The cyclohexanol-Nafion ionomer-Pt/C exhibited a lower Tafel slope (67.1 mV dec^{-1}) than the Nafion ionomer-Pt/C (72.7 mV dec^{-1}). The mass activity of cyclohexanol-Nafion ionomer-Pt/C measured at 0.85 $V_{HFR\text{-}free}$ is 1.0 A mg_{Pt}^{-1}, representing a 25% improvement relative to Nafion ionomer-Pt/C (0.80 A mg_{Pt}^{-1}). Considering the same Pt loading and the similar H_{upd}-ECSA in the two catalyst layers, the higher kinetic activity of cyclohexanol-Nafion ionomer-Pt/C should be attributed to cyclohexanol effectively releasing more active sites of Pt.

https://doi.org/10.1038/s41929-023-00949-w

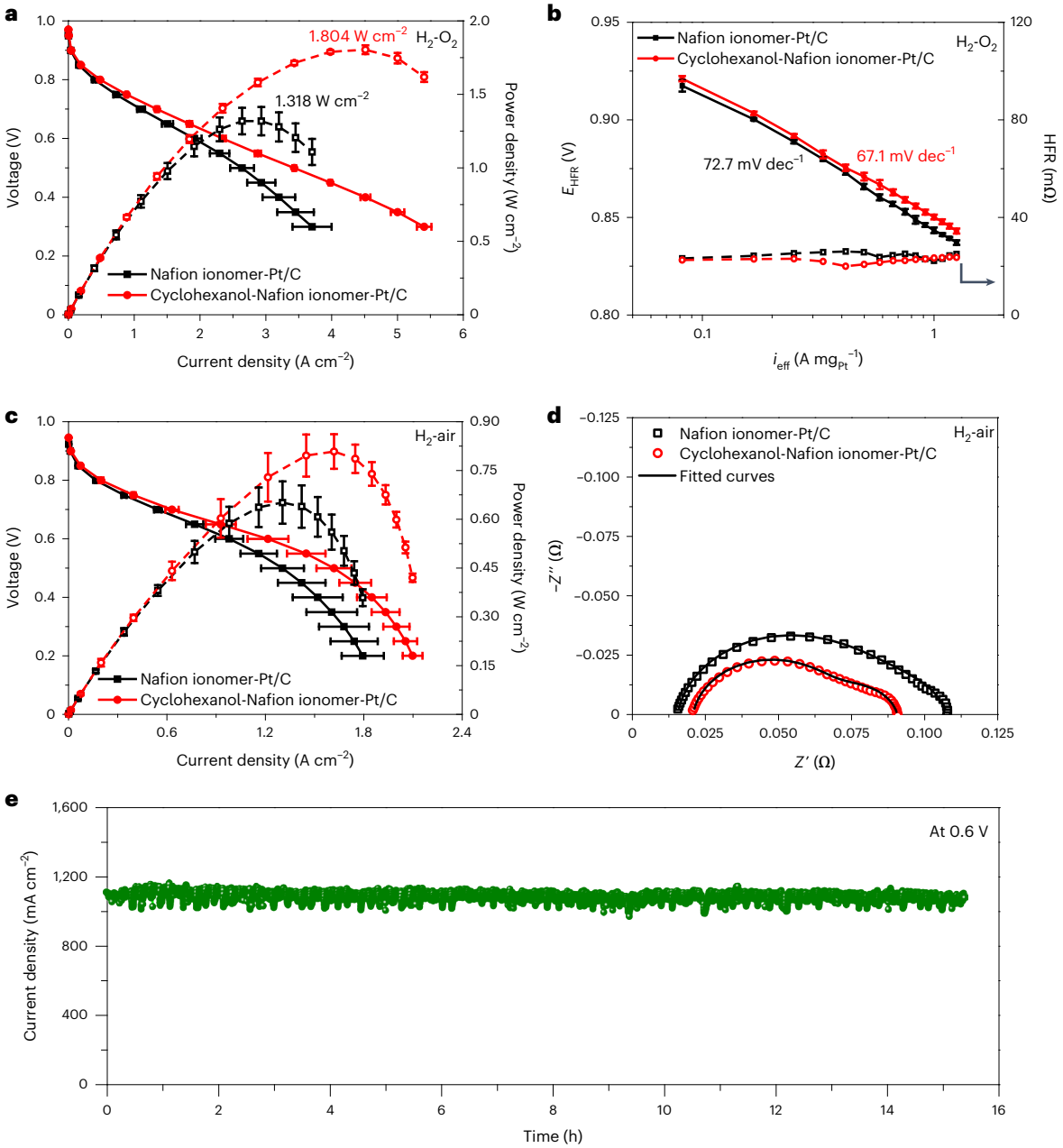

Fig. 4 | Effects of cyclohexanol incorporation on fuel-cell performance. **a**, H_2–O_2 fuel-cell performance of Nafion ionomer-Pt/C and cyclohexanol-Nafion ionomer-Pt/C catalyst layers. **b**, Tafel plots of Nafion ionomer-Pt/C and cyclohexanol-Nafion ionomer-Pt/C catalyst layers with HFR correction measured under H_2–O_2 conditions. **c**, H_2–air fuel cell performance of Nafion ionomer-Pt/C and cyclohexanol-Nafion ionomer-Pt/C catalyst layers. **d**, In situ electrochemical impedance spectroscopy curves measured at an output current density of 1 A cm^{-2} in H_2–air conditions. **e**, Stability test of the cyclohexanol-Nafion ionomer-Pt/C catalyst layer in a H_2–air fuel cell at 0.6 V. For all MEAs, the anode catalyst is Pt/C at a Pt loading of 0.08 mg_{Pt} cm^{-2}, and the cathode Pt loading is 0.12 mg_{Pt} cm^{-2}; membrane, Nafion HP; temperature, 80 °C; RH, 100%; back pressure, 200 kPa_{gauge}. For the H_2–O_2 cell, the H_2 and O_2 flow rates were fixed at 250 and 350 s.c.c.m., respectively. For the H_2–air cell, the flow rates of H_2 and air were 300 and 500 s.c.c.m., respectively. The error bar corresponds to the standard deviation between the three independent measurements. Data are presented as mean values ± s.d.

To evaluate the application potential of the cyclohexanol-Nafion ionomer-Pt/C, a H_2–air fuel cell was estimated. As shown in Fig. 4c, the cyclohexanol-Nafion ionomer-Pt/C exhibits a current density of 0.93 A cm^{-2} at 0.65 V, which is 21% higher than that of Nafion ionomer-Pt/C (0.77 A cm^{-2}). The maximum power density (0.808 W cm^{-2}) of cyclohexanol-Nafion ionomer-Pt/C is 1.24 times higher than that of Nafion ionomer-Pt/C (0.651 W cm^{-2}). This improvement in MEA performance far exceeds the results of the previously reported study of Pt/C catalysts (Supplementary Table 2), representing one of the record effective strategies. The best fitting of electrochemical impedance spectroscopy (EIS) (Fig. 4d and Supplementary Fig. 15) also highlights the decrease in both charge-transfer resistance (R_{ct}) and mass transport resistance (R_{mt}) of the cyclohexanol-Nafion ionomer-Pt/C catalyst layer. The behaviour of the reduced R_{ct} and R_{mt} verifies that cyclohexanol is favourable for releasing Pt intrinsic activity and facilitating mass transport in the catalyst layer. We also explored the stability of the cyclohexanol-Nafion ionomer-Pt/C with constant-potential testing in the H_2–air fuel cell (Fig. 4e). The cyclohexanol-Nafion ionomer-Pt/C stably worked at 0.6 V for more than 15 h without marked current-density decay. The running temperature was 80 °C, far above

the melting point of cyclohexanol. The extraordinarily stable current demonstrates that cyclohexanol remains largely present. To describe the stability of the cyclohexanol-Nafion ionomer-Pt/C in more detail, accelerated stress tests (ASTs) were performed by cycling the potential between 0.05 and 0.85 V under H_2/N_2 conditions with 100% RH at a scan rate of 50 mV s^{-1}. The cyclohexanol-Nafion ionomer-Pt/C was scanned for 30,000 cycles, and the corresponding proton sheet resistance was recorded every 10,000 cycles. As shown in Supplementary Fig. 16, the cyclohexanol-Nafion ionomer-Pt/C showed almost no change in proton sheet resistance after 30,000 potential-scanning cycles. These results demonstrate the high stability of cyclohexanol in Nafion and the positive interaction of the $COH_2^+SO_3^-$ group in the cyclohexanol-Nafion ionomer-Pt/C catalyst layer.

Conclusions

We have successfully developed an effective strategy to improve the catalytic performance of Pt in an MEA by precisely blocking Nafion's sulfonate group with cyclohexanol. ^{1}H NMR, ATR-FTIR and XPS spectra revealed a strong coordination interaction between the hydroxyl group of cyclohexanol and the sulfonate group in the ionomer. Synchrotron SAXS confirmed that cyclohexanol with different conformations led to a remarkable enhancement of the microphase separation of Nafion. Cyclohexanol effectively enhanced the kinetic activity and mass transport by reducing the coverage of the sulfonate group on the Pt surface and improving the ionomer distribution. This study has introduced a path to drive the translation of highly active ORR catalysts to efficient catalyst layers.

Methods

Chemicals and materials

We used cyclohexanol (Shanghai Titan Scientific Co., 99%+), isopropanol (Adamas, 99.8%), Nafion ionomer (D520, DuPont), Nafion membrane (HP, DuPont), carbon paper (TGP-H-060, Toray) and Pt/C catalyst (HiSPEC9100, JM-60 wt%). All chemical reagents and materials were used as received.

Cyclohexanol-Nafion ionomer and catalyst layer preparation

The cyclohexanol-Nafion ionomer was prepared by dispersing a certain amount of cyclohexanol in an isopropanol solution containing a Nafion ionomer dispersion with a 10/1 weight ratio of cyclohexanol/Nafion ionomer. The catalyst layer was fabricated by blending the Pt/C catalysts with the as-prepared cyclohexanol-Nafion ionomer. The cyclohexanol/ionomer/carbon ratio was 10/1/2.5 by weight. A conventional cathode catalyst layer without cyclohexanol incorporation was also prepared and denoted as Nafion ionomer-Pt/C. After ultrasonic treatment, the resulting catalyst layers were applied for physical characterization experiments and MEA preparation.

Physical characterization

An Agilent 400-MR DD2 spectrometer was used to detect the ^{1}H NMR spectra of different components at 400 MHz. The Nafion ionomer dispersion was dried before testing to remove interference from solvent. Samples were dissolved in an insert tube filled with DMSO-d_6. The ATR-FTIR spectra of the different components were obtained using a Nicolet iS50 spectrometer under ambient conditions. To avoid the interference of solvents in the ionomer solution, dry Nafion HP membranes were used in FTIR measurements. The samples were fixed directly on the diamond accessory of the ATR-OMNI sampler during measurements. Determination of the electronic structure (XPS tests) of the Nafion ionomer and Pt was performed in ultrahigh vacuum (UHV) at room temperature using an ESCALAB 250Xi spectrometer. All spectra were charge-corrected in accordance with the binding energy of 284.8 eV from C 1*s*. DLS measurements were performed using a NanoBrook Omni instrument (Brookhaven Instruments) to confirm the aggregate size of the catalyst slurry. All catalyst slurries were diluted to 2–3% of the raw slurry concentration to avoid multiple scattering. At least five measurements were taken to ensure the repeatability of the results. XRD was conducted to determine changes in the Pt crystalline structure within the Pt/C catalyst layer. The instrument was a PANalytical X' Pert Power system using a Cu-$K_{\alpha 1}$ (γ = 1.54051 Å) X-ray source operating at room temperature with a rate of 5° min^{-1}. Before measurements, the catalyst layer was crushed and placed on a Si wafer. A Talos F200S system (ThermoFisher Scientific) was used to capture the TEM images with an accelerating voltage of 200 kV. The catalyst slurries diluted with isopropanol were dried and deposited on a carbon-film-coated copper grid as the sample for testing. To observe the effect of cyclohexanol incorporation on the surface micromorphology of the catalyst layer, the catalyst slurry was deposited onto the HP membrane and analysed using a JEOL JSM-7800F instrument at an accelerating voltage of 5 kV. SEM results clearly showed that both catalyst layers displayed a uniform and porous surface.

Nafion membrane pretreatment

A commercially available Nafion HP PFSA membrane (thickness, 20 μm) was used for synchrotron radiation SAXS tests and conductivity experiments. Both samples were tested as received. The cyclohexanol-incorporated HP membrane (cyclohexanol-Nafion HP membrane) was prepared by immersing the Nafion HP membrane in pure cyclohexanol. For SAXS experiments, to monitor the microstructure of the HP membranes in the dry state, both the cyclohexanol-Nafion HP membrane and the pristine Nafion HP membrane were equilibrated in a dry nitrogen stream before testing. For the conductivity experiment, both membranes were rinsed with 18.2-MΩ deionized water before the experiment.

Synchrotron SAXS

To examine the effect of incorporating cyclohexanol in Nafion on its microphase separation, a SAXS test was performed at the 1W2A beamline at the Beijing Synchrotron Radiation Facility (BSRF) in China. The wavelength (λ) of the incident X-ray beam used for the test was 1.54 Å, and the distance from the dried Nafion HP membrane to the detector was 1,512 mm. The relationship between the scattered wavevector $\mathbf{q}$, beamline wavelength λ and scattering angle θ is given by

$$\mathbf{q} = (4\pi \sin\theta/2)/\lambda. \quad (1)$$

The scattering line profile is extracted by a radial integration of the 2D scattering patterns using the free official software Fit 2D.

Conductivity measurements

To determine the in-plane proton conductivity of the HP membranes, an SI 1260 (Solartron Analytical) frequency response analyser was used to perform EIS measurements. During the conductivity measurements, the HP membranes were assembled into a two-electrode cell and immersed in deionized water. The in-plane proton conductivity of the membrane was calculated as

$$\sigma = 10^7 \times l/(R_f \times \delta \times d), \quad (2)$$

where the proton conductivity σ (in mS cm^{-1}) is inversely proportional to the resistance data R_f fitted from the EIS spectra, the distance l between the two electrodes is 2 cm, and d and δ denote the width (1 cm) and thickness of the HP membrane, respectively. The two-electrode cell was operated at frequencies of 1 to 10^7 Hz and at different temperatures (from 25 to 80 °C).

The activation energy (E_a, in electronvolts) of proton conduction in the Nafion HP membrane was calculated from the Arrhenius equation:

$$\ln(\sigma T) = \ln A - E_a/RT, \quad (3)$$

where A is the preexponential factor, R is the molar gas constant (8.314 J mol^{-1} K^{-1}), and σ is the calculated proton conductivity value at temperature T (in kelvin).

Fuel-cell testing and electrochemical analysis

The cyclohexanol-Nafion ionomer-Pt/C and Nafion ionomer-Pt/C for the cathode were sprayed onto a Nafion HP membrane at a target Pt loading of 0.12 mg_{Pt} cm^{-2}. In addition, to determine the impact of a higher cyclohexanol content on cell performance, a cathode catalyst layer with a cyclohexanol/Nafion/carbon mass ratio of 40/1/2.5 was prepared. The concentrations of Nafion ionomer and the Pt loading in the cathode catalyst layer were identical for all MEAs. All anode catalyst layers were prepared with Pt/C catalyst dispersed in isopropanol solvent with a fixed Nafion ionomer/carbon value of 1.0 and a controlled Pt loading of 0.08 mg_{Pt} cm^{-2}. Once fabricated, the MEAs were assembled at a hot press pressure of 700 psi and 135 °C for 150 s. The assembled MEA was sealed into a single-cell fixture with a 5-cm^2 serpentine flow field and tested with a full-function Scribner 850e fuel cell system equipped with an 885 potentiostat (Scribner Associates). After the break-in procedure, for mass activity measurements, fully humidified (100% RH) pure H_2/O_2 was provided with a flow rate of 250/350 s.c.c.m. to minimize the effect of mass transport. The back pressure was 200 kPa_{gauge}. I–V polarization curves were obtained from the anodic scan direction with the scanning voltage mode. Test conditions were set as follows: cell temperature of 80 °C; 100% RH anode/cathode for the Pt/C catalyst layer; H_2/air flow rate of 300/500 s.c.c.m. with a back pressure of 200 kPa_{gauge}. At a cell output current density of 2.0 A cm^{-2}, the fuel flows are equivalent to a stoichiometric ratio of 4/3 for the anode/cathode. EIS analysis was conducted at a current density of 1 A cm^{-2} in a H_2/air fuel cell by a load and frequency analyser from 10 kHz to 0.1 Hz to differentiate the contribution of each impedance parameter to the total impedance. For the stability test of the H_2–air fuel cell, the anode and cathode were supplied with fully humidified H_2 (300 s.c.c.m.) and compressed air (500 s.c.c.m.) with a back pressure of 200 kP_{agauge}, respectively. The cell was operated at 80 °C. The current density points were recorded every 3 s to monitor performance changes. CVs were recorded with a potentiostat (Scribner 885-HS) in a single cell at 40 °C and 100% RH under ambient pressure, and the flow rate was 200/10 s.c.c.m. The cathode was used as the working electrode, sweeping from 0.1 to 1.2 V at 50 mV s^{-1}. By integrating the absorbed/desorbed hydrogen charge with a double-layer charging current as a baseline, Pt ECSA values in the CV were calculated with

$$\mathrm{ECSA_{CV}} = Q_{\mathrm{Pt}}/(Q_{\mathrm{ref}} \times m_{\mathrm{Pt}}), \quad (4)$$

where Q_{Pt} is the average charge of the hydrogen adsorption/desorption area, Q_{ref} = 210 μC cm^{-2} is the electrical charge generated by the oxidation of hydrogen in the monolayer on the Pt surface, and m_{Pt} is the mass of Pt loading in the cathode catalyst layer.

The $-SO_3H$ group adsorbed on the Pt surface can be displaced by linear adsorption of CO, in which the measured displacement current transient can be integrated to obtain displacement charge (q_{dis}). Therefore, the $-SO_3H$ group coverage over the Pt catalyst can be calculated via CO-displacement and CO-stripping experiments. The CO displacement and CO stripping were run in a single cell with the anode purged with hydrogen working as the reference electrode and the cathode acting as the working electrode under fully wet (40 °C) conditions at ambient pressure. The CO-displacement procedure is as follows. First, the CV procedure was performed to verify the cleanliness of the MEA. Next, a potential of 0.4 V versus RHE was applied to eliminate the negligible hydroxyl coverage until a steady current was established, then the cathode supply gas was switched from N_2 to CO (80 s.c.c.m.). During this step, a reduction current response corresponding to the displacement of the adsorbed ionomer was recorded. After linear adsorption of CO in the cathode catalyst layer, the cathode catalyst layer was purged with N_2, then subjected to a CO-stripping test from 0.05 to 1.2 V at 50 mV s^{-1}. The current–time response of CO displacement at 0.1 V versus RHE was also recorded when the applied voltage was changed to 0.1 V versus RHE. The $-SO_3H$ group coverage was then calculated by normalizing twice the CO-displacement charge at 0.4 V versus RHE to the CO-stripping charge (q_{strip}). The ECSA of the catalyst layer in CO stripping was calculated from the following equation, where q_{ref} is 420 μC cm^{-2} for the CO-stripping test:

$$\mathrm{ECSA_{COstrip}} = q_{\mathrm{strip}}/(q_{\mathrm{ref}} \times m_{\mathrm{Pt}}). \quad (5)$$

The displacement coverage was found using

$$\theta_{\mathrm{dis}} = (2q_{\mathrm{dis}})/q_{\mathrm{strip}}. \quad (6)$$

Accelerated stress testing (AST) included 30,000 voltage cycles in the range 0.05–0.85 V (versus RHE) at a scan rate of 50 mV s^{-1}. AST was performed in cyclohexanol-Nafion ionomer-Pt/C MEA at 80 °C, ambient pressure and a flow rate of 200 s.c.c.m. of 100% RH H_2/N_2 at the anode/cathode. For every 10,000 voltage cycles, the proton sheet impedance of the catalyst layer was recorded to assess the stability of the $COH_2^+SO_3^-$ group in cyclohexanol-Nafion ionomer-Pt/C. The proton sheet resistance estimated by impedance spectroscopy was measured at 80 °C and 25% RH. After equilibrating the cell for at least 30 min, a VersaSTAT 4 equipped with an impedance analyser and potentiostat was used to determine the impedance of the cell at open-circuit voltage (~0.10 V). The working electrode (cathode) was scanned from 65 kHz to 0.1 Hz at an a.c. perturbation of 15 mV.

Data availability

Data supporting the findings of this study are available from the corresponding author upon reasonable request.

References

1. Xie, M. et al. Pt-Co@Pt octahedral nanocrystals: enhancing their activity and durability toward oxygen reduction with an intermetallic core and an ultrathin shell. *J. Am. Chem. Soc.* **143**, 8509–8518 (2021).
2. Hu, Y. et al. Coplanar Pt/C nanomeshes with ultrastable oxygen reduction performance in fuel cells. *Angew. Chem. Int. Ed.* **60**, 6533–6538 (2021).
3. Li, M. et al. Lavender-like Ga-doped Pt_3Co nanowires for highly stable and active electrocatalysis. *ACS Catal.* **10**, 3018–3026 (2020).
4. Cheng, Q. et al. High-loaded sub-6-nm Pt1Co1 intermetallic compounds with highly efficient performance expression in PEMFCs. *Energy Environ. Sci.* **15**, 278–286 (2022).
5. Huang, L. et al. Boosting oxygen reduction via integrated construction and synergistic catalysis of porous platinum alloy and defective graphitic carbon. *Angew. Chem. Int. Ed.* **60**, 25530–25537 (2021).
6. Ding, H. et al. Epitaxial growth of ultrathin highly crystalline Pt-Ni nanostructure on a metal carbide template for efficient oxygen reduction reaction. *Adv. Mater.* **34**, 2109188 (2022).
7. Chong, L. et al. Ultralow-loading platinum-cobalt fuel cell catalysts derived from imidazolate frameworks. *Science* **362**, 1276–1281 (2018).
8. Kodama, K., Nagai, T., Kuwaki, A., Jinnouchi, R. & Morimoto, Y. Challenges in applying highly active Pt-based nanostructured catalysts for oxygen reduction reactions to fuel cell vehicles. *Nat. Nanotechnol.* **16**, 140–147 (2021).
9. Sun, Y. et al. Advancements in cathode catalyst and cathode layer design for proton exchange membrane fuel cells. *Nat. Commun.* **12**, 5984 (2021).

10. Xiao, F. et al. Atomically dispersed Pt and Fe sites and Pt-Fe nanoparticles for durable proton exchange membrane fuel cells. *Nat. Catal.* **5**, 503–512 (2022).
11. Fan, J. et al. Bridging the gap between highly active oxygen reduction reaction catalysts and effective catalyst layers for proton exchange membrane fuel cells. *Nat. Energy* **6**, 475–486 (2021).
12. Ahn, C. Y. et al. Differences in the electrochemical performance of Pt-based catalysts used for polymer electrolyte membrane fuel cells in liquid half- and full-cells. *Chem. Rev.* **121**, 15075–15140 (2021).
13. Doo, G. et al. Tuning the ionomer distribution in the fuel cell catalyst layer with scaling the ionomer aggregate size in dispersion. *ACS Appl. Mater. Interfaces* **10**, 17835–17841 (2018).
14. Lazaridis, T., Stühmeier, B. M., Gasteiger, H. A. & El-Sayed, H. A. Capabilities and limitations of rotating disk electrodes versus membrane electrode assemblies in the investigation of electrocatalysts. *Nat. Catal.* **5**, 363–373 (2022).
15. Kongkanand, A. & Mathias, M. F. The priority and challenge of high-power performance of low platinum proton-exchange membrane fuel cells. *J. Phys. Chem. Lett.* **7**, 1127–1137 (2016).
16. Modestino, M. A. et al. Self-assembly and transport limitations in confined Nafion films. *Macromolecules* **46**, 867–873 (2013).
17. Page, K. A. et al. Confinement-driven increase in ionomer thin-film modulus. *Nano Lett.* **14**, 2299–2304 (2014).
18. Tymoczko, J. et al. Oxygen reduction at a Cu-modified Pt(111) model electrocatalyst in contact with Nafion polymer. *ACS Catal.* **4**, 3772–3778 (2014).
19. Kodama, K. et al. Effect of the side-chain structure of perfluoro-sulfonic acid ionomers on the oxygen reduction reaction on the surface of Pt. *ACS Catal.* **8**, 694–700 (2017).
20. Ott, S. et al. Ionomer distribution control in porous carbon-supported catalyst layers for high-power and low Pt-loaded proton exchange membrane fuel cells. *Nat. Mater.* **19**, 77–85 (2020).
21. Yarlagadda, V. et al. Boosting fuel cell performance with accessible carbon mesopores. *ACS Energy Lett.* **3**, 618–621 (2018).
22. Jinnouchi, R. et al. The role of oxygen-permeable ionomer for polymer electrolyte fuel cells. *Nat. Commun.* **12**, 4956 (2021).
23. Katzenberg, A. et al. Highly permeable perfluorinated sulfonic acid ionomers for improved electrochemical devices: insights into structure-property relationships. *J. Am. Chem. Soc.* **142**, 3742–3752 (2020).
24. Doo, G. et al. Nano-scale control of the ionomer distribution by molecular masking of the Pt surface in PEMFCs. *J. Mater. Chem. A* **8**, 13004–13013 (2020).
25. Liu, H., Ney, L., Zamel, N. & Li, X. Effect of catalyst ink and formation process on the multiscale structure of catalyst layers in PEM fuel cells. *Appl. Sci.* **12**, 3776–3816 (2022).
26. Zhang, G. R., Munoz, M. & Etzold, B. J. M. Boosting performance of low temperature fuel cell catalysts by subtle ionic liquid modification. *ACS Appl. Mater. Interfaces* **7**, 3562–3570 (2015).
27. Zhang, G. R., Munoz, M. & Etzold, B. J. M. Accelerating oxygen-reduction catalysts through preventing poisoning with non-reactive species by using hydrophobic ionic liquids. *Angew. Chem. Int. Ed.* **55**, 2257–2261 (2016).
28. Wang, T. et al. Enhancing oxygen reduction electrocatalysis by tuning interfacial hydrogen bonds. *Nat. Catal.* **4**, 753–762 (2021).
29. Wu, X., Chen, N., Klok, H. A., Lee, Y. M. & Hu, X. Branched poly(aryl piperidinium) membranes for anion-exchange membrane fuel cells. *Angew. Chem. Int. Ed.* **61**, e202114892 (2022).
30. Liu, B. et al. Precise molecular-level modification of Nafion with bismuth oxide clusters for high-performance proton-exchange membranes. *Angew. Chem. Int. Ed.* **60**, 6076–6085 (2021).
31. Kunimatsu, K., Bae, B., Miyatake, K., Uchida, H. & Watanabe, M. ATR-FTIR study of water in Nafion membrane combined with proton conductivity measurements during hydration/dehydration cycle. *J. Phys. Chem. B* **115**, 4315–4321 (2011).
32. Kusoglu, A. & Weber, A. Z. New insights into perfluorinated sulfonic-acid ionomers. *Chem. Rev.* **117**, 987–1104 (2017).
33. Kusoglu, A., Dursch, T. J. & Weber, A. Z. Nanostructure/swelling relationships of bulk and thin-film PFSA ionomers. *Adv. Funct. Mater.* **26**, 4961–4975 (2016).
34. Kusoglu, A. et al. Impact of substrate and processing on confinement of Nafion thin films. *Adv. Funct. Mater.* **24**, 4763–4774 (2014).
35. Mikhailenko, S., Guiver, M. & Kaliaguine, S. Measurements of PEM conductivity by impedance spectroscopy. *Solid State Ion.* **179**, 619–624 (2008).
36. Wei, C. et al. Approaches for measuring the surface areas of metal oxide electrocatalysts for determining their intrinsic electrocatalytic activity. *Chem. Soc. Rev.* **48**, 2518–2534 (2019).
37. Yamada, H., Kato, H. & Kodama, K. Cell performance and durability of Pt/C cathode catalyst covered by dopamine derived carbon thin layer for polymer electrolyte fuel cells. *J. Electrochem. Soc.* **167**, 084508 (2020).
38. Zhou, F. et al. Solving Nafion poisoning of ORR catalysts with an accessible layer: designing a nanostructured core-shell Pt/C catalyst via a one-step self-assembly for PEMFC. *Int. J. Energy Res.* **44**, 10155–10167 (2020).
39. Li, Y., Intikhab, S., Malkani, A., Xu, B. & Snyder, J. Ionic liquid additives for the mitigation of Nafion specific adsorption on platinum. *ACS Catal.* **10**, 7691–7698 (2020).
40. Garrick, T. R., Moylan, T. E., Yarlagadd, V. & Kongkanand, A. Characterizing electrolyte and platinum interface in PEM fuel cells using CO displacement. *J. Electrochem. Soc.* **164**, F60–F64 (2017).

Acknowledgements

This study was financially supported by the National Key R&D Program of China (2020YFB1506002, S.C.), the National Natural Science Foundation of China (grant nos. 52021004 and 91834301, Z.W.; grant nos. 22178034 and 21978028, S.C.; grant no. 22108020, M.W.) and the Chongqing Talent Program (cstc2022ycjh-bgzxm0096, S.C.).

Author contributions

S.C., Z.W. and L.G. conceived of the project. S.C. directed the experimental work. S.C. and F.C. analysed the experimental data. F.C. carried out the sample synthesis, characterization, electrochemical measurements and fuel-cell tests. A.W. and M.W. helped with editing of the paper. S.C., L.G. and F.C. prepared the manuscript with feedback from the other authors.

Competing interests

The authors declare no competing interests.

Additional information

Supplementary information The online version contains supplementary material available at https://doi.org/10.1038/s41929-023-00949-w.

Correspondence and requests for materials should be addressed to Siguo Chen, Lin Guo or Zidong Wei.

Peer review information *Nature Catalysis* thanks Hany El-Sayed and the other, anonymous, reviewers for their contribution to the peer review of this work.